Submillimeter Array Technical Memorandum

Number: 48
Date: May 17, 1991
From: Colin Masson

Comparison of Atmospheric Opacity at Mount Graham and Mauna Kea

Summary

The results for the first continuous year of opacity measurements on Mauna Kea are presented and discussed. The analysis of available measurements on Mount Graham is also presented and contrasted. The data show that the available time with low opacity is 2 times greater at Mauna Kea than at Mount Graham, essentially because the summer monsoon season in the Southwest is not suitable for observing. While this conclusion depends on the slightly uncertain conversion between opacity and PWV, a comparison with other data suggests that our adopted conversion is, if anything, conservative, in the sense that it minimizes the difference between the two sites. Comparison of the NOAO infrared opacity measurements at Mauna Kea and Mount Graham shows a factor of 2-3 advantage for Mauna Kea at low levels of opacity, confirming our conclusion. The difference between the two sites is large enough that secondary factors such as length of periods of low opacity need not be considered in deciding between them.

Diurnal effects are well known to be large on Mauna Kea. However, the diurnal effects are quite small when the opacity is low and the wet layers of the atmosphere are well below the summit. Excellent observing weather can occur at all times of day. Seasonal effects at Mount Graham are dramatic, with summer observing prevented entirely by the monsoon weather, while seasonal effects at Mauna Kea are negligible.

1 Introduction

The high frequency performance of the SAO submillimeter array (SMA) depends critically on the atmospheric opacity at the chosen site. Even small quantities of precipitable water vapor (PWV) create significant opacity at the highest operating frequencies. Two sites are being considered for the SMA, Mauna Kea in Hawaii, with an elevation of 4200 m, and Mount Graham in Arizona, with an elevation of 3300 m. In both cases, the interferometer sites would be about 100-200 m below the peak. In this memo, I discuss the tests of opacity which have been made at the two sites and compare the results.

On Mauna Kea, the opacity has been measured since August 1989 with a 225 GHz radiometer developed by NRAO (Owen and Hogg, 1989). Scattered measurements are available in the literature for other periods (Westphal 1974, de Zafra *et al.* 1983, Parrish *et al.* 1987). Radiosonde

data can also be used to study long term trends. Mount Graham was measured by R. Martin at the University of Arizona during 1986-1987 and radiosonde data have been used to extend these measurements to a longer average (Martin 1989). For confirmation, an indirect but independent comparison can also be obtained by using measurements of infrared sky emissivity made by NOAO in the course of their site survey for the NNTT (Merrill and Forbes 1987).

2 Methods of Measurement

The opacity in the submillimeter wave windows is dominated by the PWV. The atmospheric oxygen and water lines are broadened typically by ~2 GHz at the altitudes of both our potential sites (p = 600 - 700 mbar). Most astronomical observations are necessarily made in 'windows' many line-widths away from the centers of the strong lines; the opacity in these windows is due to a superposition of wings of distant strong lines. In general, the line shapes are not known *a-priori* to sufficient accuracy to predict the opacity in the windows, so most models assume a simple mathematical lineshape, such as the van Vleck-Weisskopf function, and then add an empirical continuum term to match the measured opacity in some atmospheric window(s) (e.g. Liebe 1989, Cernicharo 1985). These models have not been accurately verified in the submillimeter windows, and one of the significant results of the SAO site-testing effort has been to collect data at different frequencies from observers on Mauna Kea and compare them with the 225 GHz opacity measured simultaneously by the NRAO machine to improve our knowledge of the opacity in the mm and submm windows (Masson 1990).

Since the atmospheric lines are pressure-broadened, the strength of the line wings increases with atmospheric pressure. Under dry conditions and when the frequency of interest is many line-widths away from the center, the opacity of the water lines can be shown to be nearly proportional ep, where p is the atmospheric pressure and e is the partial pressure of water, while the oxygen line opacity is proportional to p^2. The empirical continuum term of Liebe (1989) is also essentially proportional to ep under dry conditions. There are other terms which depend on such things as the possible water dimers, but for our purposes these are not important, since they are small under dry conditions. The water vapor in the atmosphere is concentrated at low elevations, with a rough 'scale-height' of ~2km, so it is a good approximation to say that the opacity at any given site depends on the pressure at that site and the PWV above it.

From our measurements at Mauna Kea, the opacity due to water vapor in the several windows appears to vary in direct proportion to PWV, with a small offset due to oxygen opacity, which is significant only below ~400 GHz. Table 1 gives a summary of the opacity ratios as deduced from measurements on Mauna Kea over the past year, updated from Masson (1990). The scale factors between the different windows are better determined than is the ratio between any one and the PWV.

The values in the table are probably accurate to about 10%. The oxygen opacity at the higher frequencies is not well determined, but is not significant in comparison with the water opacity. At lower altitudes the water opacities increase in proportion to the atmospheric pressure, and the oxygen opacity is proportional to the square of the pressure.

Table 1. Opacity ratios at Mauna Kea

Frequency (GHz)	Oxygen opacity nepers	Water opacity (nepers/mm)
230	0.01	0.04
345	0.07	0.10
460	-	0.56
680	-	0.80
880	-	0.80

From this discussion, it is apparent that the 225 GHz opacity measured by the NRAO tipper is closely related to the opacity which affects the operation of a submillimeter telescope. Little interpretation is therefore required to make use of the results. On Mount Graham, the opacity has been measured by a different system. This uses a 22 GHz radiometer tuned to a water line. The opacity in this line is much less than that at higher frequencies, but this is compensated for by the greater sensitivity of the receiver. Unlike the submillimeter windows, the opacity at 22 GHz varies *inversely* with pressure, since increased pressure broadens the line and reduces its strength at the center. In practice, however, this difference does not give rise to any significant complications in calibration, since the water has a small scale height. The calibration of both the 22 GHz and 225 GHz radiometers has been compared with radiosonde measurements taken at similar times and nearby locations and found to be satisfactory, within about 10% (Martin 1989, Schwab and Hogg 1988). A second NRAO 225 GHz radiometer has been measuring another high peak in the southwest, South Baldy in New Mexico.

A third type of system has been used both on Mauna Kea and Mount Graham to test the infrared properties of the sites. This is an infrared sky brightness monitor, operating at 20 and 27 μm (Merrill and Forbes 1987). It has been used only at night and only at times when the sky was relatively cloudless, but the results represent the only case in which identical machines were used for testing both sites. The infrared opacity also depends mainly on water vapor and pressure, but it is quite sensitive to temperature and may not be simply proportional to the submillimeter opacity. Nevertheless, the infrared data provide a useful check on the radio measurements.

Finally, radiosonde data are available for locations close to both sites. These give humidity as a function of elevation, which can be integrated to get PWV, but are insensitive to PWV < 2-3 mm, and to conditions local to the mountain sites.

3 Measurements on Mauna Kea

The NRAO 225 GHz radiometer has operated fairly reliably during the first year it was on Mauna Kea. There was a period during early 1990 when the original machine became faulty, after which it

was replaced by another device. The erroneous readings were edited out of the dataset, and hourly means were calculated. Figure 1 shows a histogram of the fraction of hours for which the radiometer data were available versus month of the year during the 1 year period from 1989 September - 1990 August. This fraction is not corrected for the periods when the radiometer was measuring opacity fluctuations. These periods lasted for 4096 seconds and occured every 5 hours. Depending on the exact timing of these periods, the maximum coverage of the hourly medians varies between 80% and 100%. The total coverage was 72% during this period. There is no correlation between monthly median opacity and uptime, suggesting that the down times did not bias the results.

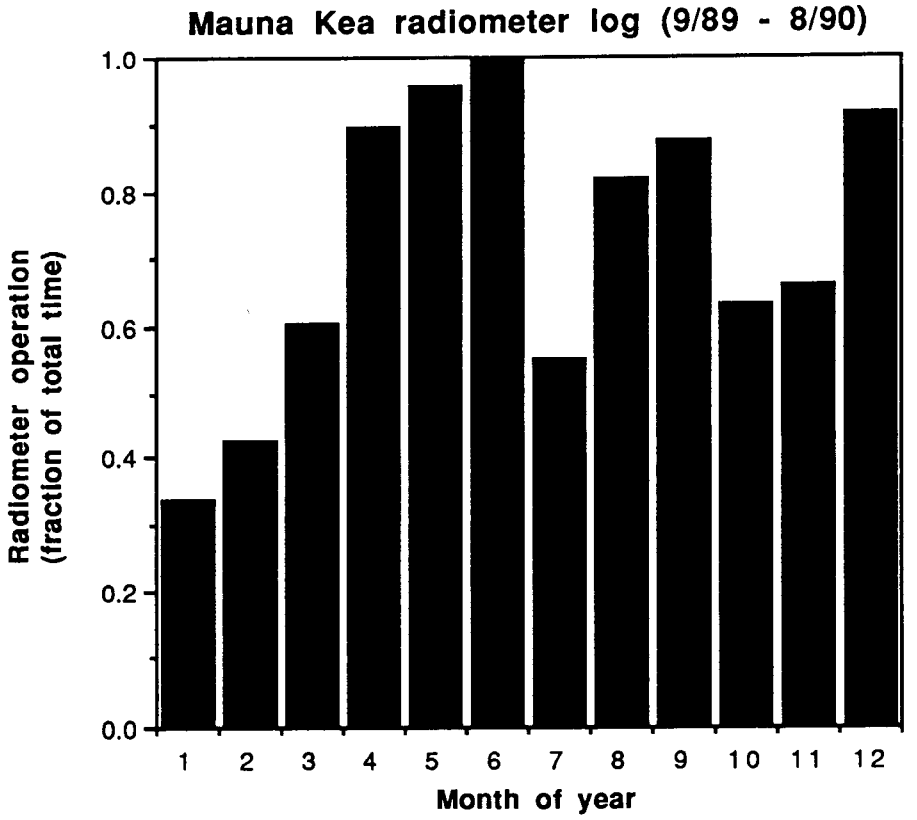

Figure 1. Fraction of time when the 225 GHz radiometer was operational for each month of the year, starting from September 1989 and ending in August 1990. The horizontal axis shows month of the year, running from January to December.

A summary of the results for the entire period on Mauna Kea is plotted in Figure 2. The measurements were edited to remove occasional bad points and the distribution was then truncated at an opacity of 0.5, before calculating the hourly medians. All further analysis is based on those medians. During the 1-year period of measurement, the overall median opacity was 0.10 and the lowest recorded values were slightly less than 0.03. Only 10% of the points have a value less than 0.05, which corresponds to 1mm of PWV. The median value was the same for the winter when the first machine was in use, as for the summer when the replacement machine was in use, consistent with the expected lack of seasonal variation.

Two other sets of measurements on Mauna Kea are also plotted in Figure 2. The first, labelled

Westphal meter, are taken from daytime infrared measurements made by Westphal (1974) over a period of one year. They have been converted from PWV to opacity at 225 GHz using the values given in Table 1. The data of Westphal show excellent agreement with the 225 GHz data. However, when account is taken of the fact that the days at Mauna Kea are worse than the nights, the Westphal data show somewhat better conditions. The other set of measurements, labelled *de Zafra radiometer*, are taken from the compilation of ~90 days and nights of observations on Mauna Kea presented by de Zafra *et al.* (1983) and Parrish *et al.* (1987), as collated by Biretta (1989). Rather than using the conversion to PWV employed by these authors, we have taken their opacities and converted them from the measurement frequency near 280 GHz to opacities at 225 GHz, using the atmospheric data of Zammit and Ade (1981). After this scaling, the data taken from de Zafra *et al.* agree fairly well with the 225 GHz measurements, but they also show better conditions.

The good agreement between the 3 sets of measurements presented in Figure 2, demonstrates that the period of our 225 GHz survey is typical of conditions on Mauna Kea, or perhaps slightly worse than average. Analysis of more recent 225 GHz radiometer data by Schinckel (private communication) also show better conditions than in the 1 year considered here. We use the 225 GHz radiometer measurements in the site comparison below.

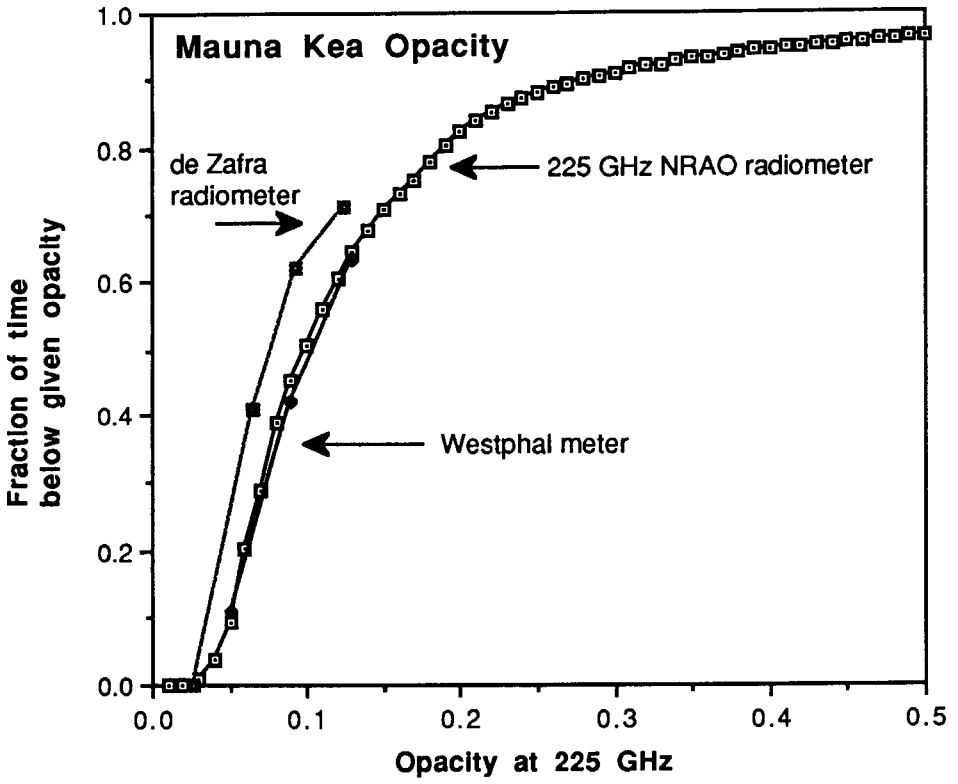

Figure 2. Distribution of opacity at 225 GHz on Mauna Kea. The vertical axis shows the fraction of time when the opacity is lower than the given opacity.

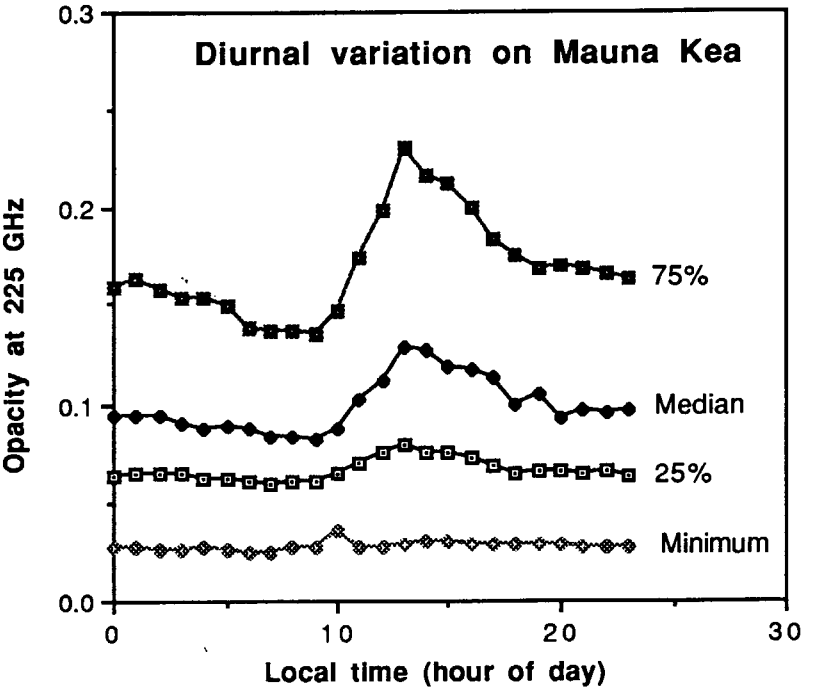

Figure 3. Diurnal variation of opacity on Mauna Kea. The lines plotted show the quartiles of the opacity distribution and the minimum observed opacity as functions of local time. There is a clear increase in opacity in the middle of the day. The diurnal variation is greatest at larger opacities, and there is little variation in the minimum observed opacity with hour of the day.

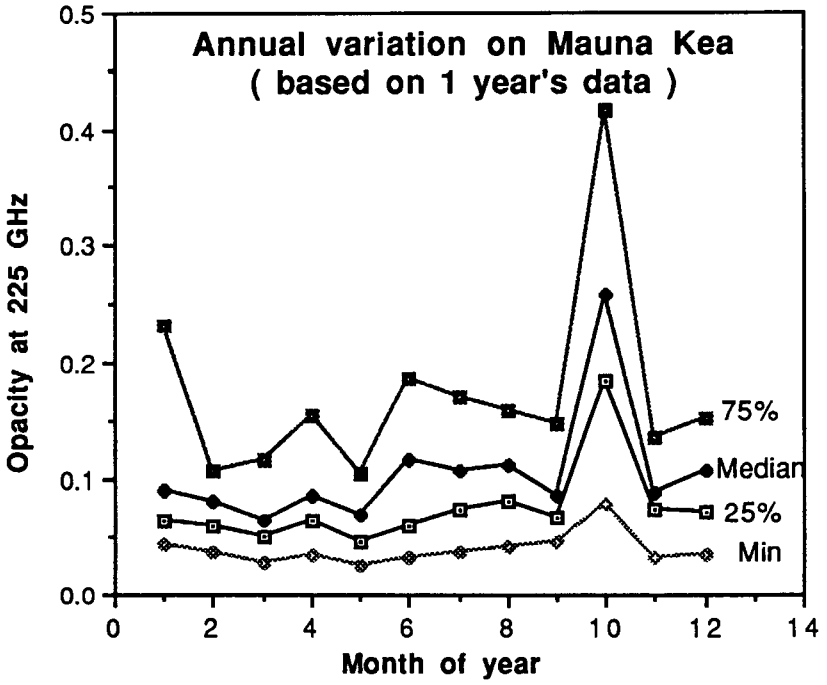

Figure 4. Annual variation of opacity on Mauna Kea. Curves plotted as in Figure 3. There is little evidence for any seasonal variation, except for a period of very bad weather in October.

There is a substantial diurnal variation of opacity on Mauna Kea. During the very best days, with night-time opacity less than 0.05, the day-time opacity is also excellent, but on worse days, the diurnal variation is larger. This effect is shown in Figure 3, which shows the median and quartile values as a function of hour of the day. Good observing conditions can occur at all times of day. Figure 4 shows a similar plot of opacity as a function of month. It can be seen that there is no significant seasonal variation, although the month of October 1989 had very bad weather.

4 Measurements on Mount Graham.

The information available for Mount Graham is considerably less complete, but we have used pre-publication radiometer data from R. Martin of the University of Arizona, in conjunction with radiosonde data provided courtesy of R. Martin and NRAO, to assess the site quality. Figure 5 shows two estimates of the annual distribution of water vapor. The U of A estimates are taken from the information provided by Martin (1989) and are based purely on radiosonde data, while the SAO estimate (Biretta 1989) uses a combination of radiosonde and radiometer data.

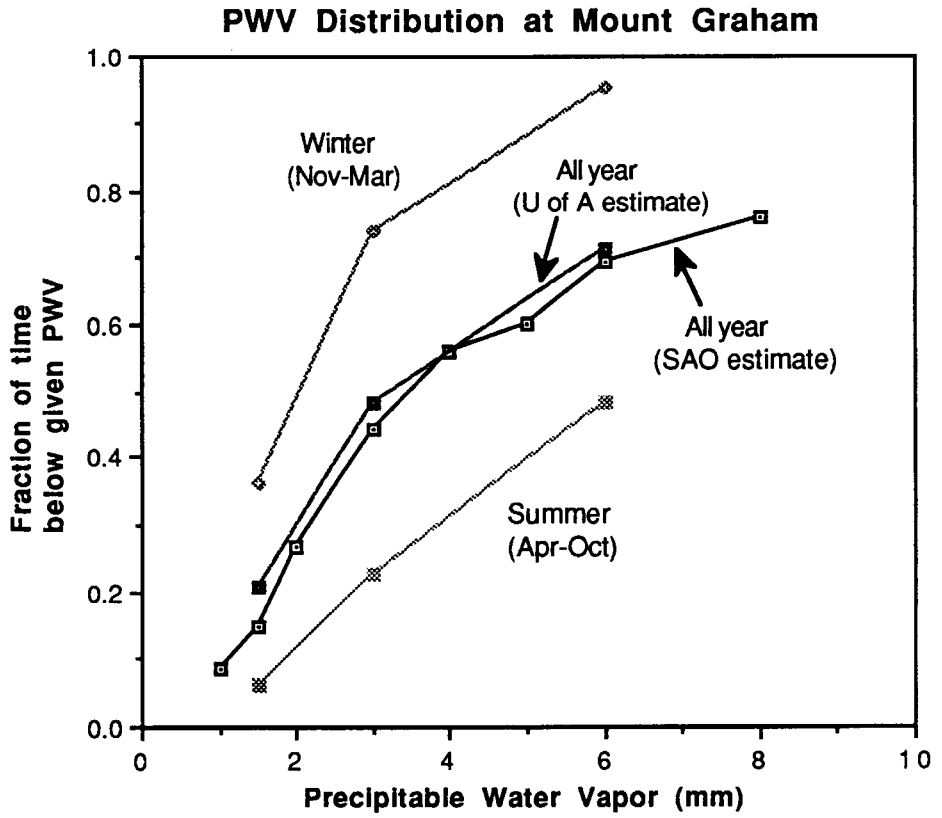

Figure 5. Distribution of PWV on Mount Graham. Both sets of curves are based on long-term radiosonde data for PWV > 2.5 mm and use an extrapolation for PWV < 2.5 mm. For this extrapolation the University of Arizona curves use a fraction of the maximum possible humidity while the SAO curve uses some direct measurements from the University of Arizona 22 GHz radiometer. The summer and winter curves are from the U of A.

The radiosondes cannot measure humidity below 19%, resulting on a lower limit of approximately 2.5 mm PWV, so the points for lower values than this are based on an extrapolation. In the curves from the University of Arizona, the extrapolation assumes that the unmeasured humidity takes half its maximum possible value, an assumption which has been statistically validated by comparison

with data from the 22 GHz radiometer. In the SAO analysis, a more complicated extrapolation has been made by Biretta (1989), based on a detailed comparison between radiosonde data and radiometric data from a two month period in early 1986. The two curves agree well, as they should, where they overlap; the extension to low values of PWV in the SAO analysis is based primarily on the radiometer data. In the following section we use the SAO analysis of the data, although we also present the Arizona version.

5 Comparison of the Sites

To put these Mount Graham values on the same scale as those for Mauna Kea, we must convert to 225 GHz opacity. The opacity at Mount Graham (p = 690 mbar) should be 11% higher than that at Mauna Kea (p = 620 mbar) for the same quantity of water vapor. We therefore use the following relation for Mount Graham, based on the values in Table 1:

$$\tau_{225} = 0.01 + 0.045 \times PWV_{mm}.$$

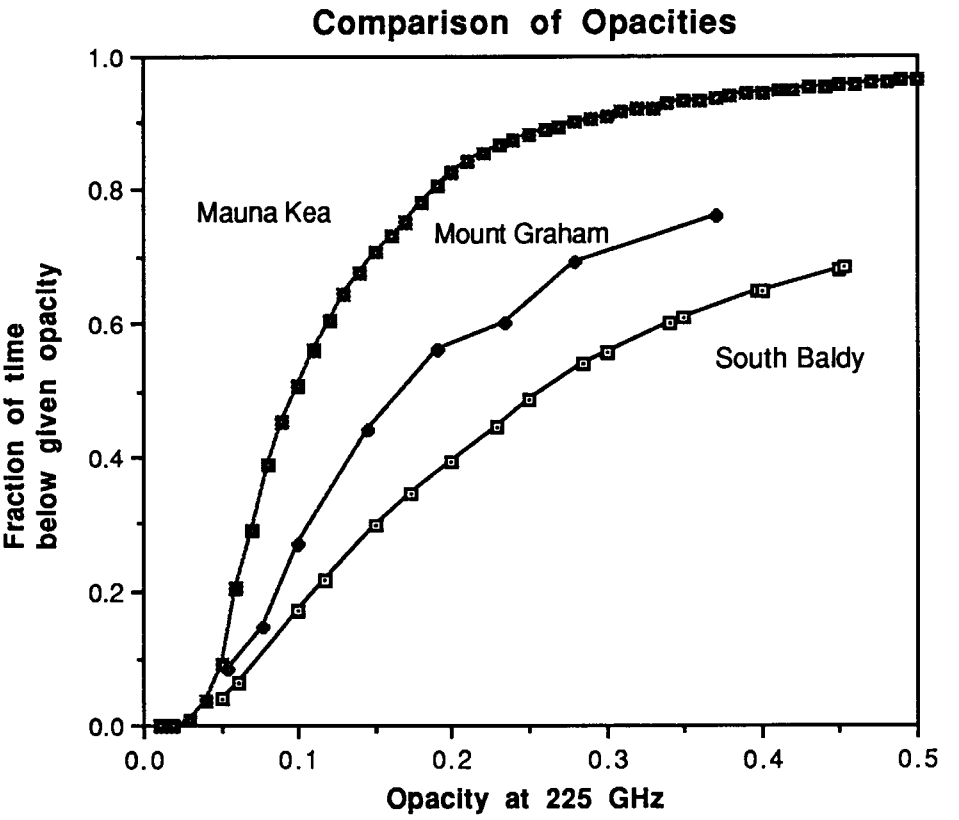

Figure 7. Distribution of opacities for the two sites under consideration, with South Baldy as a comparison. Mauna Kea and South Baldy were measured directly in terms of 225 GHz opacity, while the PWV data from Mount Graham were converted according to the formula in the text.

Figure 7 shows the Mount Graham data plotted on the same scale of 225 GHz opacity as those from Mauna Kea, with direct opacity measurements from a second southwest site, South Baldy in New Mexico, shown for comparison (Hogg, Owen and McKinnon 1988). The elevation of South

Baldy, 10500 ft, is nearly identical with that of Mount Graham, although Mount Graham is farther from the moist air associated with the Gulf of Mexico.

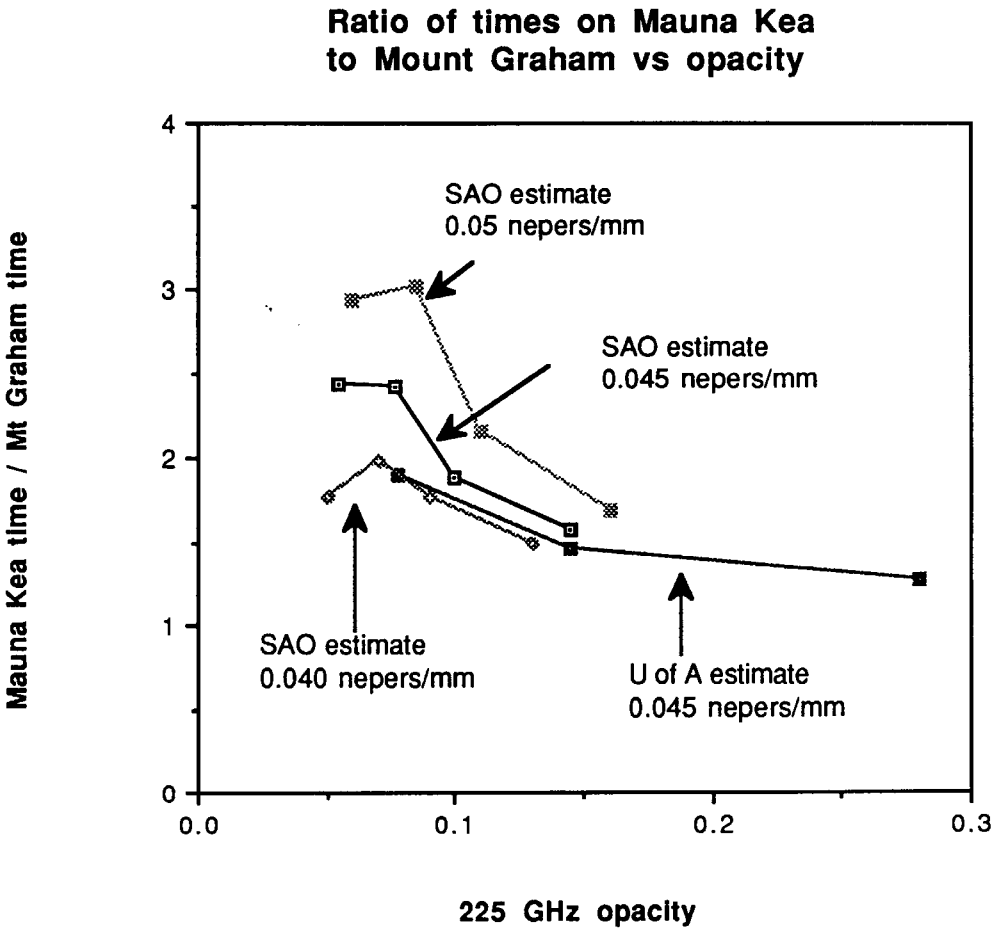

Figure 8. Ratio of time available on Mauna Kea to that available on Mount Graham as a function of opacity.

The data are plotted a different way in Figure 8, as the ratio of available time on Mauna Kea to that at Mount Graham, as a function of 225 GHz opacity. In this figure, we also present the ratio based on the University of Arizona estimate of Mt Graham opacity, and ratios showing the effect of assuming different conversions between PWV and opacity. At the critical low opacities, Mauna Kea provides a factor of approximately 2 more time than Mount Graham.

The information presented in Figures 7 and 8 shows a clear advantage for Mauna Kea over Mount Graham. However, the magnitude of this advantage depends on the assumed value for the conversion between opacity and PWV. If the conversion factor were less than 0.045 nepers/mm, then the difference between the two sites would be less. A comparison of measured opacity and average PWV at S. Baldy has been presented by Schwab and Hogg (1988). Apart from the winter months, where the PWV may be systematically overestimated due to the deficiency of the radiosondes, the best match seems to be given by a ratio slightly higher than our 0.045 nepers/mm. It is extremely unlikely that the value could be any lower than 0.045 nepers/mm. However, these pieces of evidence are indirect and we choose to maintain our originally adopted value of 0.045 until a better calibration becomes available. This is a conservative choice in the sense of minimizing the apparent difference between the properties of the two sites. The higher value of 0.05 would increase the apparent superiority of Mauna Kea.

This result is confirmed by the comparisons of radiosonde data for the two sites, which have been made by Biretta (1989) and Merrill and Forbes (1987). Further, indirect, confirmation for the comparison can be sought in the infrared sky brightness measurements made by NOAO for their site survey (Merrill and Forbes 1987). Figure 9, which is a plot of the distribution of 27 μm opacity for Mauna Kea and Mount Graham, shows a substantial difference between the two sites, again in favor of Mauna Kea by a factor of 2-3. The distribution has been truncated at an emissivity corresponding to 8% of the time at Mount Graham, so that it is comparable with the range of data presented in Figure 8.

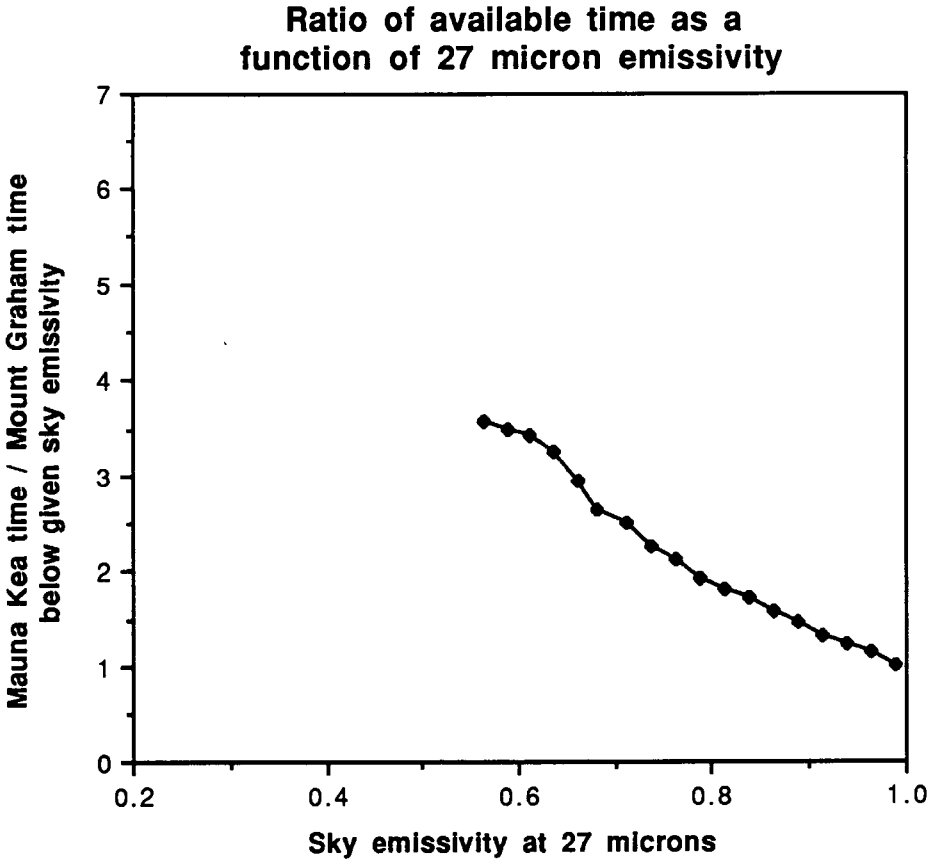

Figure 9. Ratio of available times on Mauna Kea and Mount Graham, as a function of 27 μm sky emissivity (from NOAO data).

6 Conclusion

The comparison shows that Mauna Kea has a significant advantage over Mount Graham in the time available at low opacity. This advantage is large enough that it will not be affected by any possible sampling error or calibration in the data. Other measurements and long-term radiosonde information show that the datasets we have used for the comparison are representative of conditions on the two sites. An assessment of calibration uncertainty suggests that any bias is conservative, in the sense of underestimating the opacity at Mount Graham and minimising the difference between the two sites. In view of the clear advantage provided by Mauna Kea, there is no need to consider secondary characteristics of the opacity.

Acknowledgements

I thank Bob Martin for providing samples of his radiometer and radiosonde data in advance of publication, and for comments on an earlier version of this report, and Frazer Owen, John Biretta, and Richard Hills for helpful discussions.

References

Biretta, J. A. 1989. *A preliminary study of radiometer data for Mauna Kea, Mt. Graham, and South Baldy*. SMA Technical Report.

Cernicharo, J. 1985. *ATM: A program to compute theoretical atmospheric opacity for frequencies <1000 GHz*. IRAM Internal Report 15.4.85

de Zafra, R. L., Parrish, A., Solomon, P. M., and Barrett, J. W. 1983. Int'l. J. IR & MM Waves **4**, 757.

Hogg, D. E., Owen, F. N., and McKinnon, M. 1988. *First results from the site-testing program of the millimeter-wave array*. NRAO Millimeter Array Memo No. 45.

Liebe, H. J. 1989. Int'l. J. IR & MM Waves **10**, 631.

Martin, R. N. 1989. private communication.

Masson, C. R. 1990. *Atmospheric Opacity and Water Vapor*. SMA Technical Memo No. 12.

Merrill, K. M. and Forbes, F. F. 1987. *Comparison Study of Astronomical Site Quality of Mount Graham and Mauna Kea*. NNTT Technology Development Program Report No. 10, NOAO.

Owen, F. N. and Hogg, D. E. 1989. NRAO preprint.

Parrish, A., de Zafra, R. L., Barrett, J. W., Solomon, P., and Connor, B. 1987. Int'l. J. IR & & MM Waves **8** 431.

Schwab, F. R. and Hogg, D. E. 1988. *Millimeter-Wave Seeing Inferred from Radiosonde Observations - Preliminary Results*. NRAO Millimeter Array Memo No. 51.

Westphal, J. A. 1974. *Infrared Sky Noise Survey* Final report NASA grant NGR 05-002-185.

Zammit, C. C. and Ade, P. A. R. 1981. Nature **293**, 550.

JET PROPULSION LABORATORY

INTEROFFICE MEMORANDUM
OSAS DFM # 91-59
PSR DFM # 91-68
April 16, 1991

TO: Distribution

FROM: E. B. Hochberg, K. Wallace

SUBJECT: PSR Prototype Panel Optical Figure Testing:
Room & cold temperature figure tests of **HR4m1** on 4/11/91.

PSR PANEL OPTICAL TEST REPORT SUMMARY

OPTICAL TEST PERSONNEL	K. Wallace
TEST DATE	~~1/17/91~~ 4/11/91
PANEL DESIGNATION	**HR4m1**
PANEL SHAPE; SIZE	hexagonal; 0.892 m point-to-point
PANEL HISTORY/PREPARATION	see text

AS-MANUFACTURED ROOM-TEMPERATURE FIGURE

PANEL AREA MEASURED:	~98% (a few localized drop-outs)	
ABS. RADIUS OF CURVATURE:	ROC = 7.600 m ±12 mm @ T_{amb} = 10 C	
AS-MFG'D. SURF. PRECISION @ ROC:	RMS @ T_{amb}	= 2.857 μm
SEIDEL ABERRATIONS:	Astigmatism	= 1.206 waves
	Coma	= 0.433 waves
	Spherical	= -0.475 waves

COLD TEMPERATURE FIGURE STABILITY

PANEL TEMPS & GRADIENTS	T_{amb}	= 10 C;
	T_{min}	= -40 C = 233 K;
	max gradient	= 25 C
DEFORMATIONS vs. TEMPERATURE	RMS @ T_{min}	= 8.69 μm
	$\Delta RMS_{total}/\Delta T$	= 0.162 μm/C
	$\Delta Z3/\Delta T$	= -0.054 waves/C
LONG-TERM FIGURE CHANGE	not measured	

REFERENCES

See previous HR-series test reports: JPL OSAS DFM 's #90-100, #90-101, #90-102 and #91-16 (HR-4).

PREFACE

This report includes certified test results obtained with the 10.59 micron phase-shifting interferometer as integrated in the AFAL cryointerferometric test facility. See OSA DFM #90-50 (PSR DFM #90-45) entitled PSR Panel Optical Testing: Ambient and Thermal Optical Figure Tests of SYS-6 on 6-7-90 and 7-2-90 dated July 6, 1990 for a detailed description of the optical test system and standardized test procedures.

TEST PERSONNEL & ATTENDEES:

Optical testing under room & cold temperature conditions of "one meter" prototype panel HR-4 was conducted on 4/11/91: Conducting the test from JPL were: K. Wallace (Sect. 385), T. Hill (Sect. 355) and J. McGregor (Sect. 354).

ENVIRONMENTAL & TEST CONDITIONS

Room & cold temperature figure tests on 4/11/91 were conducted from 11 am to 10 pm. Ambient temperature inside the completed interferometer room was a stable 22 C with the enclosure air-conditioner (heating) running. Winds outside the hanger were negligible throughout the test; atmospheric conditions are described as "windy, cool, clear".

REPLICATION TOOL DESCRIPTION

replication tool ROC	7.485 m ±1.0 mm (sphereometer)
tool aperture	1.0 meter
tool quality	RMS < 0.5 micron (estimate)

MIRROR DESCRIPTION

designation	**HR4m1**
shape	hexagonal
size	0.8255 m flat-to-flat, 0.891 m point-to-point f/8.55
release film	spray-on organic release
facesheet material	Celion G30-500/F151 or C6000F155
front facesheet design	12 ply; 38 microns co-cured aluminum on top
front surface preparation; appearance	co-cured aluminum; specular,
rear facesheet ROC	same as front
core material, thickness, design	aluminum, 89 mm, "single flexcore"

MIRROR HISTORY

date	location	test performed/activity
?	~~JPL~~ done by Hexcel	mounting holes drilled thru back facesheet
1/17/91	AFAL	thermal test down to -24 C = 249 K

OPTICAL FIGURE AT ROOM TEMPERATURE: ABSOLUTE RADIUS OF CURVATURE:

See **Figure 1.** Absolute radius of curvature (ROC) measurement per the technique described in OSA DFM #90-71 (PSR DFM #90-47) was performed for this panel. The ROC measurement of 1/17/91 was **7.621 meters,** very similar to the other HR panels; measurement on this date is **7.600 meter.** Given the error in measurement is estimated to be ±0.5 inch (±12 mm) actual ROC may not have changed at all, or as much as 45 mm. (See **Figure 2** for a bar chart summary of absolute ROC measurements collected to date.)

OPTICAL FIGURE MEASUREMENTS UNDER ROOM TEMPERATURE CONDITIONS:

This panel bears a fairly strong resemblance to the other HR panels measured in November of 1990. Qualitatively, the surface exhibits a high spatial frequency "waffle pattern". The hexagonal aperture is well-defined with only a handful of small-area dropouts over the aperture in the vicinity of the most extreme, small, high-slope areas (particularly in front of the holes drilled in the back of the rear facesheet).

Common test conditions:

test date:	4/11/91
panel average temperature:	10 C
vacuum:	yes
interferometer lens:	f/8
pupil image magnification:	1X
PEV (detector) sampling:	256 pixels x 256 pixels
data sampling for Zernike polynomial fitting :	256 x 256 (entire data set)
data area:	133 x 143 pixels
pixel size on test aperture:	0.891 m/119pixels = 7.5 mm

Five measurements are acquired at room temperature and under rough vacuum. Removing piston, tilt & focus from each measurement, the average is:

HR4m1VacAvg = 2.857 μm @ T = 10 C; rough vacuum.

The figure above is reported for HR4m1 room temperature "as-manufactured surface precision compared to best-fit radius of curvature".

See **Figure 5** for a tabulation of room temperature as-manufactured RMS surface precision at best-fit center of curvature for all panels measured to date.

ZERNIKE SURFACE DECOMPOSITION

See **Figure 3** for a tabulation of Zernike coefficients, Seidel aberrations and other surface statistics for the room-temperature as-manufactured surface; data collected on 4/11/91. These results refer to an average of five measurements collected with the panel under vacuum.

Total RMS surface error may be broken down into "low" and "high" spatial frequency components: "Low" spatial frequency refers to that portion of the total surface deformation described by 33 lowest-order Zernike coefficients (not including Z1, Z2, or Z3: two tilts and one focus coefficient.) These Zernikes describe a surface with no more than six "inflection points" or cycles per aperture.

The "high" spatial frequency portion is the RMS error of the surface remaining after the first 36 Zernike surfaces are removed from the total. Wireframes, contour maps & surface profiles of the total average surface and it's low & high spatial frequency components are shown in **Figure 4.**

Note the pyroelectric vidicon detector in the interferometer limits spatial resolution to no more than about 50 cycles per aperture. Results (in microns) from the 1/17/91 and 4/11/91 tests are tabulated below.

	RMS, microns	
	1/17/91	4/11/91
(1) Total surface	2.839	2.857
(2) surface composed 1st 36 Zernikes	2.716	2.634
(3) surface after removal of 1st 36 Zernikes	0.819	1.099
RSS of (2) and (3)	2.836	2.854

Note surface peak-to-valley is 21.18 microns, 7.4 times the RMS value of the surface.

SEIDEL SURFACE DESCRIPTION

The low spatial frequency Seidel surface deformations (derived from the Zernike coefficients) are tabulated below:

Seidel Aberrations:

Astigmatism = 1.206 waves; Coma = 0.433 waves; Spherical = -0.475 waves.

Figure 6 shows residual RMS fit error as a function of Zernike term order number for room temperature, as-manufactured PSR panel surfaces. Note the largest improvement obtains in going from a 2nd order fit (just tilt & focus) to a 4th order fit which includes lowest order astigmatism, coma & spherical Zernike aberrations. Diminishing improvement in fit is seen as more terms are included. However, rather than asymptotically approaching zero fit error, approximately 0.1 waves or 1.0 micron RMS of residual error remains even after fitting terms to 12th order for the "average panel". This is attributed to real high spatial frequency errors (frequencies greater than six cycles over the aperture represented by the highest Zernike and 50 cycles per aperture detector Nyquist limit.) Conclusion: Zernike polynomials are limited in their ability to analytically describe surface figure of PSR mirrors out to spatial frequencies limited by detector Nyquist.

OPTICAL FIGURE MEASUREMENTS UNDER COLD TEMPERATURE CONDITIONS:

Figure 7 shows 10 panel thermocouple outputs, calculated average temperature & maximum temperature gradient versus time for this cold test. Note gas-only cooling was used for this test instead of circulating liquid nitrogen which is faster but typically produces larger gradients. However, gas-only cooling proceeded so slowly (more than 2 hours to go from -3C to -40C) that time forced testing to be terminated after the collection of only nine figure measurements.

Note top-to-bottom temperature difference ("gradient") across the panel increases from 15 to 23C as the panel temperature is lowered.

As in the previous test, the interferometer was longitudinally shifted twice in order to follow the large panel ROC change. Five measurements were taken in the starting position, two in a second position, and the last two in a third position.

Figure 8 is the six-page spreadsheet containing all thermo-optical data from the cold temperature figure test of HR4m1.

See **Figure 9** in which the Zernike terms Z3 to Z8 are plotted vs. panel average temperature. As usual, change in Z3 predominates as temperature is lowered. Z3 alone vs. temperature is plotted in **Figure 10**. From the first five data points (fixed interferometer) we find slope is 0.054 waves/C compared to 0.055 waves/C measured on 1/17/91.

In **Figure 11** we plot change in total RMS vs. temperature. Again, considering only the first five measurements for which the interferometer was fixed, we find dRMStotal/dT =0.162 microns/C.

Figure 12 shows thermal stability (total RMS vs. temperature) measurements to date.

LIST OF FIGURES

Distribution: (32 copies)

JPL

J.	Breckinridge	169-314
D.	Carmel	168-314
M.	Chrisp	169-214
E.	Cohen	168-327
D.	Coulter	67-201
A.	Deslis	179-111
R.	Freeland	157-507
T.	Glavich	169-314
S.	Gulkis	169-506
R.	Helms	158-103
G.	Helou (IPAC)	100-22
T.	Hill	158-103
H.	Kadogawa	169-214
C.	Kuo	157-316
M.	Levine	169-214
S.	Macenka	169-314
M.	Mahoney	168-327
J.	McGregor	157-316
A. & M.	Meinel	169-314
N.	Nerheim	23-1
N.	Page	179-111
G.	Parks	T-1182
C.	Porter	158-103
D.	Rapp	157-316
D.	Redding	198-326
G.	Sevaston	198-326
M.	Shao	169-214
A.	Vaughan	179-225
K.	Wallace	169-214
P.	Willis	157-507

JPL Collaborators

Prof. William F. Hoffmann
Steward Observatory, University of Arizona
Tucson, Arizona 85721

Mr. Pete Turner
HEXCEL Structural Products
11711 Dublin Blvd.
Dublin, CA 94568

FIGURE 1:
SCHEMATICALLY SHOWING MEASUREMENT
of ABSOLUTE ROC of PSR PANELS

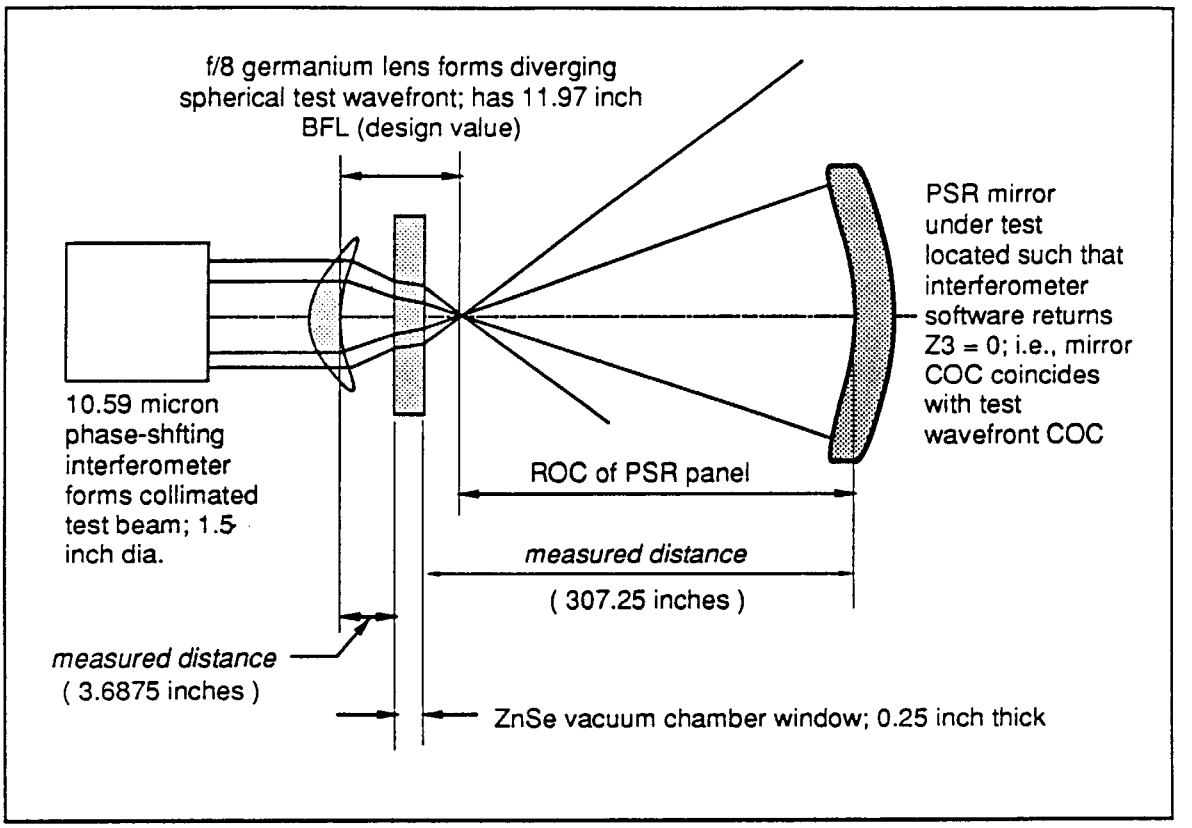

ROC of HR4M1on 4/11/91 = 307.25 + 0.25 + 3.6875 - 11.97 = 299.2175 in = 7.600 meters

Figure 2: Absolute radius of curvature measurements as of 4/11/91

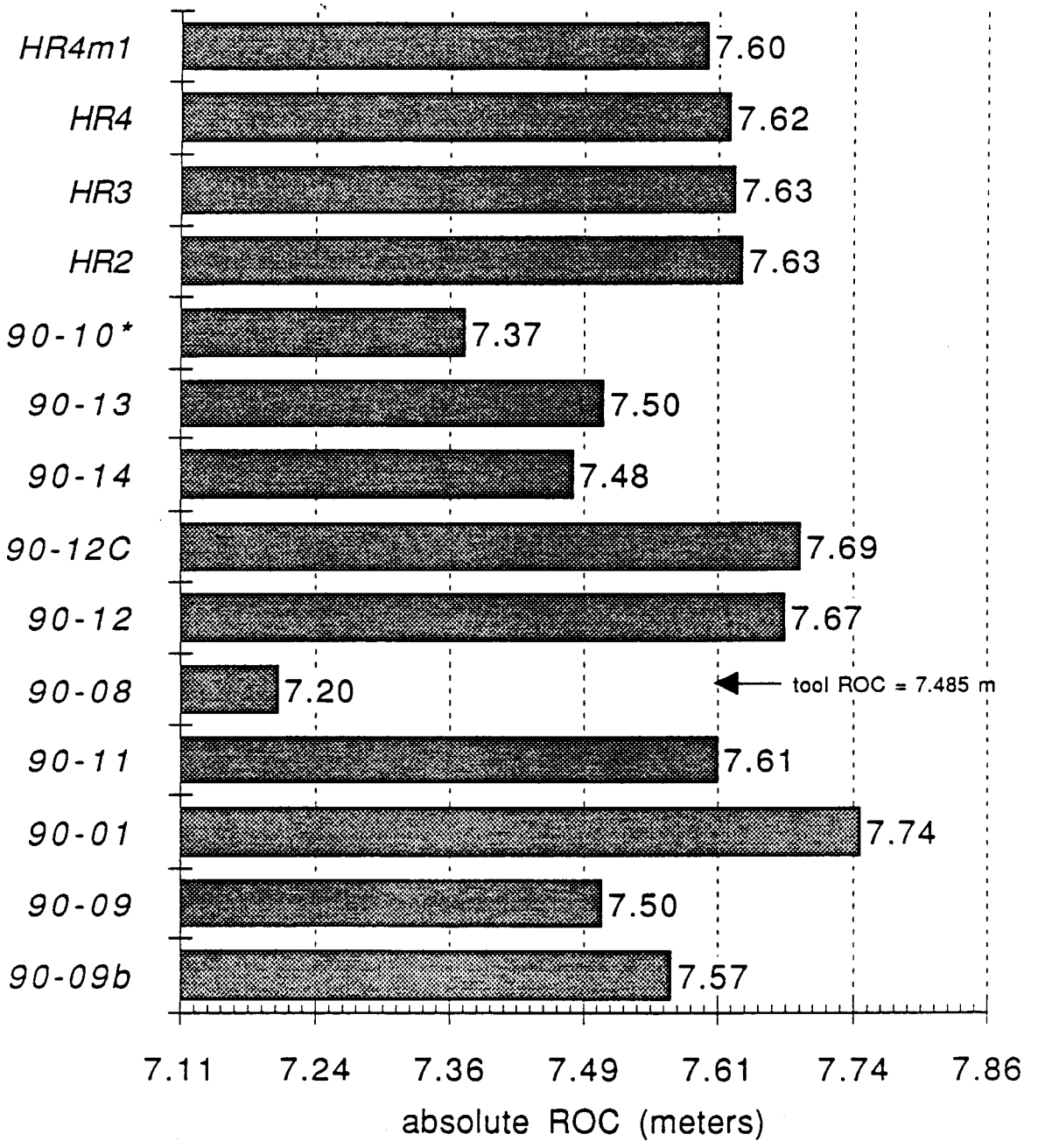

Isys-Engineering Hi-res 386 0.92 Breault Research Organization, Inc.

File: G:\HR4M1\HR4M1\VACAVG.OPD, Fri Apr 12 14:09:31 1991

	Tilt	Focus	Astig.	Coma	Spher.
	1) 0.000	3) -0.000			
2nd	2) -0.000				
	RMS fit: 0.270		4) 0.401	6) 0.011	8) -0.079
4th	RMS fit: 0.129		5) -0.450	7) -0.144	
			11) -0.041	9) -0.010	15) -0.042
			12) 0.139	10) -0.166	
				13) 0.037	
6th	RMS fit: 0.131			14) -0.080	
			16) 0.154	18) 0.070	24) -0.034
			17) 0.150	19) -0.190	
			20) -0.014	22) -0.124	
8th	RMS fit: 0.113		21) 0.081	23) -0.047	
			27) 0.065	25) 0.036	35) 0.017
			28) 0.060	26) -0.116	
			31) -0.054	29) -0.067	
			32) 0.020	30) -0.103	
				33) -0.011	
10th	RMS fit: 0.104			34) -0.010	
12th	RMS fit: 0.104				36) -0.011

Path : D:\
File : VAC
Title:

Isys-Engineering Hi-res 386 0.92 Breault Research Organization, Inc.

Seidel coefficients

File: G:\HR4M1\HR4M1\VACAVG.OPD, Fri Apr 12 14:09:59

	Magnitude	Angle
Tilt:	0.288	47.260
Focus:	-0.129	
Astigmatism:	1.206	-12.079
Coma:	0.433	-42.733
Spherical:	-0.475	
Peak - Valley:	2.000	
RMS:	0.270	
Strehl ratio:	0.057	
Wavelength:	10.590	

Number of points used for fit: 9389
Zernike Unit Circle: Inscribed

Isys-Engineering Hi-res 386 0.92 Breault Research Organization, Inc.

Data Width:	119	pixels	
Data Height:	129	pixels	
Waves Per Fringe:	0.500		
Peak to Valley:	2.000	waves,	21.180 microns
Peak:	0.943	waves,	9.990 microns
Valley:	-1.061	waves,	-11.231 microns
RMS:	0.270	waves,	2.857 microns
Strehl:	0.057		
Average:	0.012	waves,	0.131 microns
Wave length:	10.590	microns	
Pixel Sample Ratio:	1.080		
Number of Points:	9391		
Aberrations Removed:	Piston	Tilt	Focus

Path : D:\ISYS
File : VACAVG
Title:

FIGURE 3

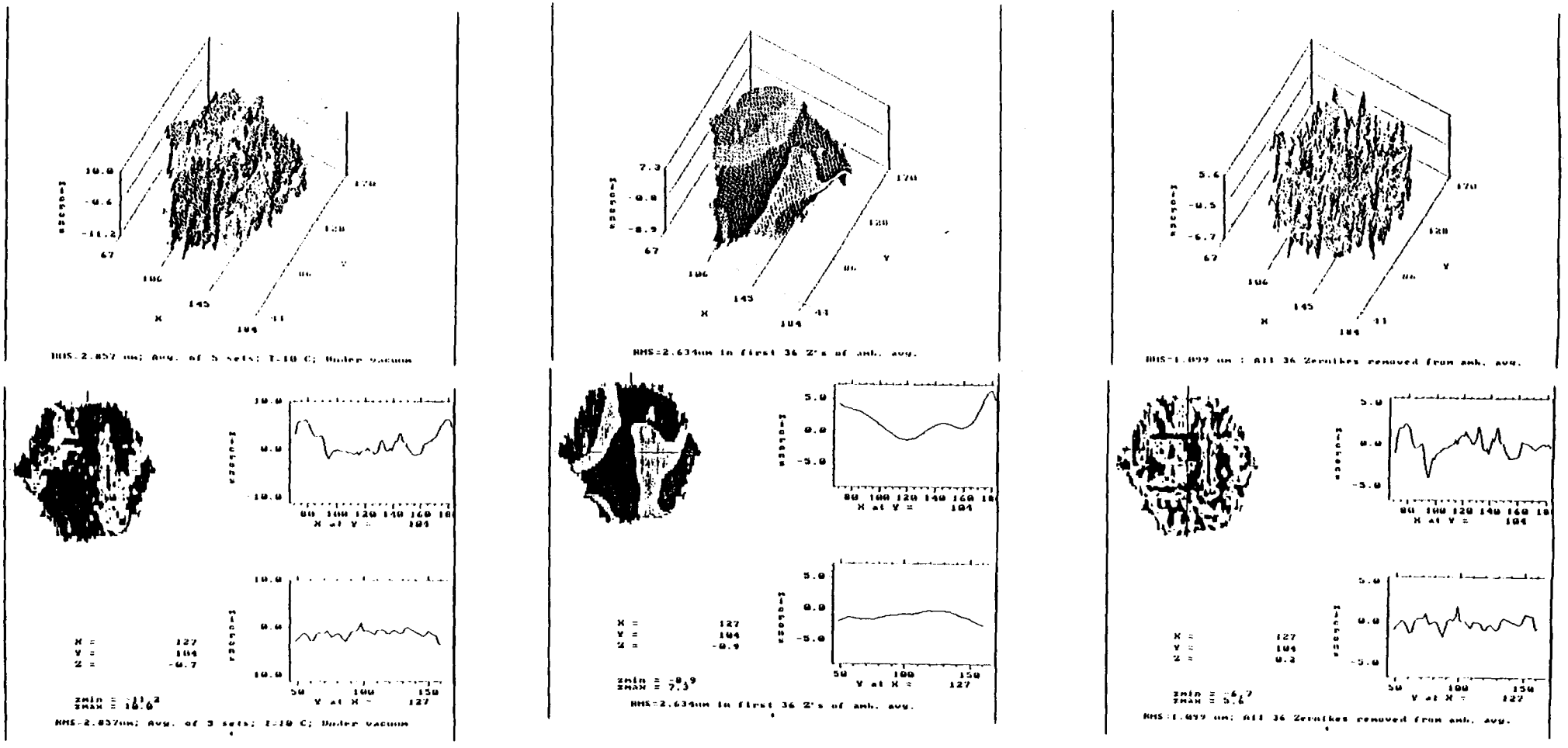

FIGURE 4

Figure 5: PSR Panels as of 4/11/91: ROOM-TEMPERATURE AS-MFG. SURF. PRECISION at BEST-FIT COC

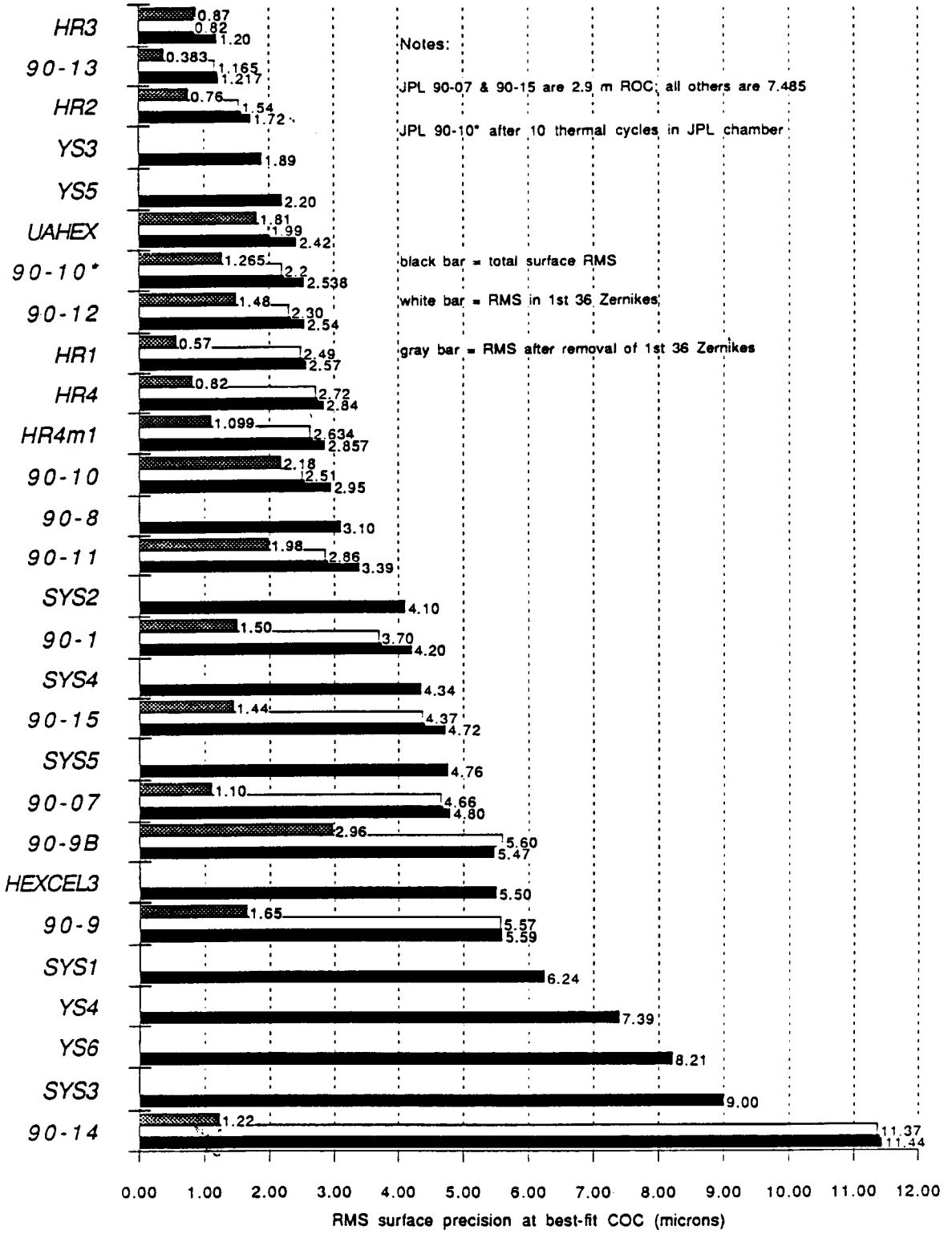

FIGURE 6

PANELS TESTED to 4/11/91: ROOM-TEMPERATURE
FIGURE - FIT ERROR by ZERNIKE ORDER NUMBER

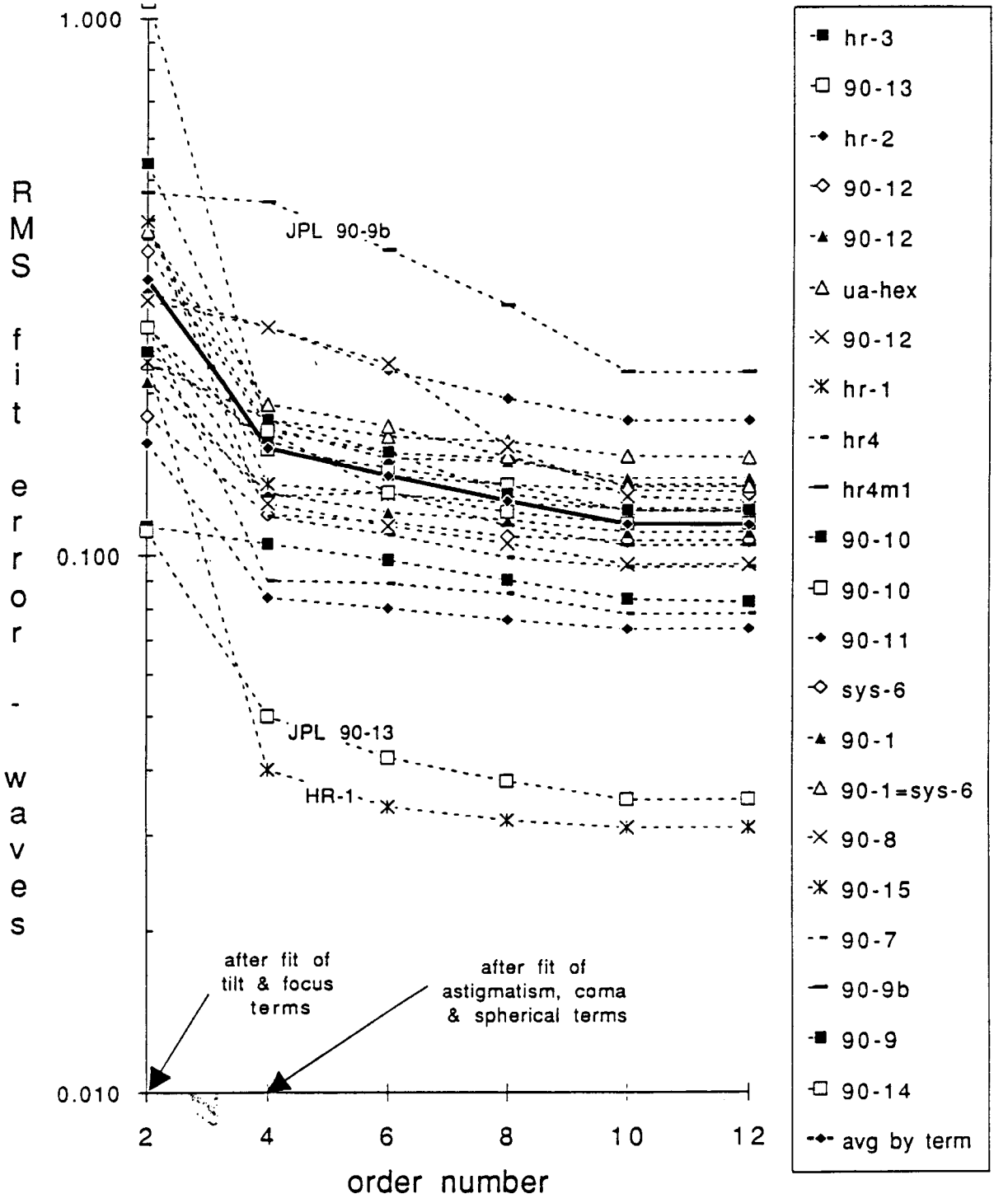

FIGURE 7

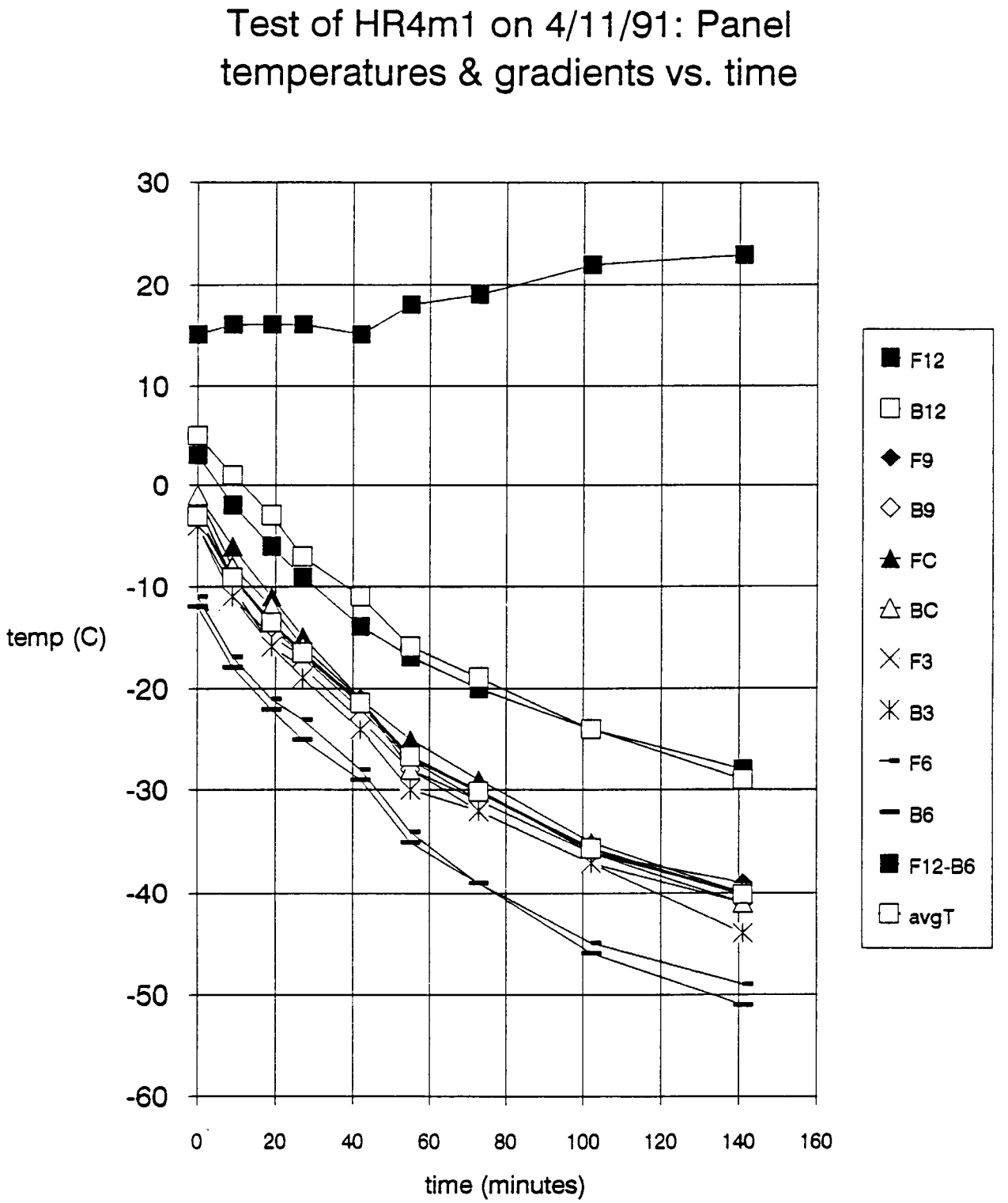
Test of HR4m1 on 4/11/91: Panel temperatures & gradients vs. time
temp (C)
30
20
10
0
-10
-20
-30
-40
-50
-60
0
20
40
60
80
100
120
140
160
time (minutes)
F12
B12
F9
B9
FC
BC
F3
B3
F6
B6
F12-B6
avgT

FIGURE 8

	M	N	O	P	Q	R	S	T	U	V	W	X	Y	Z	AB	AC	AD	AE	AF	AG	AH	AI	AJ	AK	AL	AM
21																		RMS fit error, waves								
22														////				B16	C17	C21	C25	C31	C32		B14	C15
23	Tme	F12	B12	F9	B9	FC	BC	F3	B3	F6	B6	F12-B6	avgT		Inde	avgT	Me:	2nd	4th	6th	8th	10th	12th	avgT	Z1	Z2
24	0	3	5	-2	-4	-1	-1	-4	-4	-11	-12	15	-3.1		3	-3.1	T1	0.29	0.14	0.13	0.11	0.10	0.10	-3	-0.269	0.005
25	9	-2	1	-9	-10	-8	-8	-11	-11	-17	-18	16	-9.1		61	-9.1	T2	0.29	0.15	0.14	0.13	0.10	0.10	-9	-0.382	-0.198
26	19	-6	-3	-14	-16	-11	-12	-15	-16	-21	-22	16	-13.6		119	-13.6	T3	0.32	0.16	0.15	0.14	0.11	0.11	-14	-0.221	-0.033
27	27	-9	-7	-17	-18	-15	-16	-17	-19	-23	-25	16	-16.6		177	-16.6	T4	0.31	0.16	0.15	0.14	0.11	0.11	-17	0.030	0.165
28	42	-14	-11	-21	-23	-21	-21	-22	-24	-28	-29	15	-21.4		235	-21.4	T5	0.33	0.19	0.15	0.15	0.11	0.11	-21	-0.430	0.065
29	55	-17	-16	-27	-28	-25	-28	-27	-30	-34	-35	18	-26.7		293	-26.7	T6	0.29	0.16	0.14	0.13	0.11	0.11	-27	-0.341	0.038
30	73	-20	-19	-30	-32	-29	-31	-31	-32	-39	-39	19	-30.2		351	-30.2	T7	0.32	0.16	0.14	0.13	0.11	0.11	-30	-0.372	-0.109
31	102	-24	-24	-36	-37	-35	-36	-36	-37	-45	-46	22	-35.6		409	-35.6	T8	0.31	0.15	0.14	0.13	0.11	0.11	-36	-0.108	0.048
32	141	-28	-29	-39	-41	-40	-41	-40	-44	-49	-51	23	-40.2		467	-40.2	T9	0.32	0.17	0.14	0.13	0.11	0.11	-40	-0.229	0.161
33															525											
34															583											
35															641											
36															699											
37															757											
38															815											
39															873											
40															931											
41															989											
42															##											
43															##											
44															##											
45															##											
46															##											
47															##											
48															##											
49															##											
50															##											
51															##											
52															##											
53															##											
54															##											
55															##											
56															##											
57															##											
58															##											
59															##											
60															##											
61															##											
62															##											
63															##											
64															##											
65															##											
66															##											
67															##											
68															##											
69															##											
70															##											
71															##											
72															##											
73															##											
74															##											

	AN	AO	AP	AQ	AR	AS	AT	AU	AV	AW	AX	AY	AZ	BA	BB	BC	BD	BE	BF
21																			
22	D14	D16	E17	F16	G17	H16	D18	D19	B18	B19	B20	E21	F18	B22	B23	D22	D23	B24	E25
23	Z3	Z4	Z5	Z6	Z7	Z8	Z9	Z10	Z11	Z12	Z13	Z14	Z15	Z16	Z17	Z18	Z19	Z20	Z21
24	-0.112	0.484	-0.533	0.074	-0.157	-0.125	-0.008	0.044	-0.017	0.066	0.087	-0.080	-0.063	0.007	0.082	0.118	-0.147	-0.089	0.090
25	0.082	0.485	-0.536	0.063	-0.119	-0.163	-0.029	0.187	-0.004	0.033	0.057	-0.054	-0.045	0.017	0.118	0.033	-0.033	-0.027	0.124
26	0.393	0.564	-0.488	0.099	-0.174	-0.238	-0.062	0.063	0.013	0.164	0.092	-0.121	-0.072	0.012	0.151	0.055	-0.173	-0.025	0.111
27	0.584	0.565	-0.459	0.130	-0.134	-0.255	-0.058	0.125	-0.012	0.155	0.114	-0.074	-0.054	-0.019	0.166	0.023	-0.065	0.016	0.109
28	0.831	0.602	-0.841	0.206	0.095	-0.240	-0.131	0.591	0.073	-0.111	0.118	0.007	-0.037	0.052	-0.164	-0.068	0.177	0.035	-0.064
29	-0.019	0.439	-0.512	-0.026	-0.090	-0.163	0.016	0.186	0.035	0.142	0.049	-0.030	-0.006	-0.021	0.208	0.058	-0.107	-0.064	0.087
30	0.208	0.691	-0.584	-0.115	-0.151	-0.129	-0.038	0.264	0.137	0.095	-0.078	-0.071	0.045	-0.059	0.065	-0.004	-0.015	0.085	0.089
31	-0.193	0.590	-0.587	-0.083	0.006	-0.137	-0.080	0.318	-0.036	0.004	0.058	0.061	0.006	0.079	0.142	0.075	0.022	-0.152	0.044
32	-0.117	0.609	-0.601	-0.104	-0.026	-0.153	-0.071	0.376	0.008	-0.003	0.075	0.026	-0.032	0.081	0.020	0.032	0.036	-0.152	0.062
33																			
34																			
35																			
36																			
37																			
38																			
39																			
40																			
41																			
42																			
43																			
44																			
45																			
46																			
47																			
48																			
49																			
50																			
51																			
52																			
53																			
54																			
55																			
56																			
57																			
58																			
59																			
60																			
61																			
62																			
63																			
64																			
65																			
66																			
67																			
68																			
69																			
70																			
71																			
72																			
73																			
74																			

	BG	BH	BI	BJ	BK	BL	BM	BN	BO	BP	BQ	BR	BS	BT	BU	BW	BX	BY
21																SEIDEL ABERRATIO		
22	D24	G25	F22	D26	D27	B26	B27	D28	D29	B28	B29	B30	E31	F26	E32	B38	C38	B39
23	Z22	Z23	Z24	Z25	Z26	Z27	Z28	Z29	Z30	Z31	Z32	Z33	Z34	Z35	Z36	TLTma	TLTang	focus
24	-0.129	-0.016	-0.059	0.049	-0.156	0.088	0.016	-0.117	-0.059	-0.070	0.080	0.065	-0.005	0.016	-0.037	0.524	71.3	-0.195
25	-0.106	-0.027	-0.060	0.031	-0.202	0.162	-0.009	-0.194	-0.005	-0.061	0.050	0.071	-0.016	0.019	-0.020	0.510	87.8	0.418
26	-0.046	-0.047	-0.096	0.003	-0.289	0.167	0.026	-0.167	-0.085	-0.068	0.073	0.058	0.006	-0.010	-0.015	0.525	71.6	1.466
27	-0.054	-0.025	-0.099	0.018	-0.317	0.137	0.004	-0.174	-0.037	-0.123	0.050	0.052	0.027	0.044	-0.014	0.490	59.1	1.967
28	-0.114	0.029	-0.050	-0.001	-0.161	0.206	-0.161	-0.267	0.037	-0.016	0.058	0.012	0.015	0.054	-0.029	0.851	-85.8	2.069
29	-0.102	-0.022	-0.078	0.033	-0.232	0.164	0.077	-0.142	0.045	-0.107	0.038	0.049	0.027	0.016	-0.014	0.362	71.5	0.265
30	-0.187	-0.039	-0.040	0.044	-0.262	0.127	-0.006	-0.163	0.006	-0.033	0.055	-0.019	0.001	0.036	-0.006	0.240	83.1	0.288
31	-0.119	0.031	-0.040	-0.058	-0.216	0.154	0.068	-0.085	0.046	-0.153	0.018	0.009	0.031	0.028	-0.040	0.069	15.8	-0.396
32	-0.162	-0.030	-0.075	0.045	-0.126	0.132	-0.029	-0.162	0.067	-0.142	0.034	-0.009	0.037	0.045	-0.024	0.214	47.9	-0.174
33																		
34																		
35																		
36																		
37																		
38																		
39																		
40																		
41																		
42																		
43																		
44																		
45																		
46																		
47																		
48																		
49																		
50																		
51																		
52																		
53																		
54																		
55																		
56																		
57																		
58																		
59																		
60																		
61																		
62																		
63																		
64																		
65																		
66																		
67																		
68																		
69																		
70																		
71																		
72																		
73																		
74																		

	BZ	CA	CB	CC	CD	CE	CF	CG	CH	CI	CJ	CK	CL	CM	CN	CO	CP	CQ	CR	CS
21	N COEFFICIENTS derived from Zs												STATISTICS AFTER Z ABERRATION REMOVAL							
22	B40	C40	B41	C41	B42	B43	B44	B45	B46	B47	B48		B67	B55	B56	B57	B58	B66	D61	
23	Amag	Aang	Cmag	Cang	spheri	PVmic	rawRMS	Strhl	wvl	fit pts	Zcircle	Z	rsmrd	wth	hi pi	wv/f	PVmic	pts	avgT	RMSmic
24	1.441	-11.9	0.520	-32.3	-0.749	2.113	0.318	0.02	10.59	8993	Inscrib	iston	Tilt	119	129	0.5	19.298	8993	-3.1	3.085
25	1.446	-12.0	0.404	-31.0	-0.976	2.369	0.347	0.01	10.59	8989	Inscrib	iston	Tilt	119	129	0.5	21.263	8989	-9.1	3.156
26	1.492	-10.2	0.601	-30.1	-1.426	2.117	0.405	0.00	10.59	8544	Inscrib	iston	Tilt	119	129	0.5	20.766	8544	-13.6	4.200
27	1.455	-9.8	0.560	-22.9	-1.527	2.203	0.468	0.00	10.59	8452	Inscrib	iston	Tilt	119	129	0.5	22.711	8452	-16.6	4.863
28	2.068	-13.6	0.680	12.4	-1.442	2.820	0.571	0.00	10.59	8569	Inscrib	iston	Tilt	119	129	0.5	28.233	8570	-21.4	5.908
29	1.350	-12.3	0.280	-53.0	-0.978	2.180	0.321	0.02	10.59	8771	Inscrib	iston	Tilt	119	129	0.5	20.518	8775	-26.7	3.100
30	1.809	-10.0	0.570	-63.6	-0.776	2.213	0.352	0.01	10.59	8436	Inscrib	iston	Tilt	119	129	0.5	20.001	8436	-30.2	3.653
31	1.665	-11.2	0.250	88.0	-0.823	1.980	0.316	0.02	10.59	8499	Inscrib	iston	Tilt	119	129	0.5	20.808	8499	-36	3.323
32	1.711	-11.2	0.321	-82.9	-0.916	2.137	0.329	0.01	10.59	8518	Inscrib	iston	Tilt	119	129	0.5	20.704	8518	-40	3.302
33																				
34																				
35																				
36																				
37																				
38																				
39																				
40																				
41																				
42																				
43																				
44																				
45																				
46																				
47																				
48																				
49																				
50																				
51																				
52																				
53																				
54																				
55																				
56																				
57																				
58																				
59																				
60																				
61																				
62																				
63																				
64																				
65																				
66																				
67																				
68																				
69																				
70																				
71																				
72																				
73																				
74																				

	CT	CU	CV	CW	CX	CY	CZ	DB	DC	DD	DE	DF	DG	DH	DI	DJ	DK
21																	
22						Z1,Z2 rem'd											
23	Zrem'd	avgT	RMSmic	linRMS	avgT	RMSmic	linRMS	F12	avgT	Z3	linZ3	Z4	linZ4	Z5	linZ5	Z6	linZ6
24	Z1toZ3	-3.1	3.09	2.677	-3.1	3.085	3.97	##	-3.1	-0.112	-0.16	0.484	0.50	-0.533	-0.53	0.074	0.15
25	Z1toZ3	-9.1	3.16	3.649	-9.1	3.156	3.93	##	-9.1	0.082	0.16	0.485	0.52	-0.536	-0.54	0.063	0.11
26	Z1toZ3	-13.6	4.20	4.379	-13.6	4.200	3.90	##	-14	0.393	0.40	0.564	0.53	-0.488	-0.55	0.099	0.08
27	Z1toZ3	-16.6	4.86	4.865	-16.6	4.863	3.88	##	-17	0.584	0.56	0.565	0.54	-0.459	-0.56	0.130	0.06
28	Z1toZ3	-21.4	5.91	5.643	-21.4	5.908	3.85	##	-21	0.831	0.82	0.602	0.56	-0.841	-0.57	0.206	0.03
29	Z1toZ3	-26.7	3.10	6.501	-26.7	3.100	3.81	##	-27	-0.019	1.10	0.439	0.58	-0.512	-0.58	-0.026	0.00
30	Z1toZ3	-30.2	3.65	7.069	-30.2	3.653	3.79	##	-30	0.208	1.29	0.691	0.59	-0.584	-0.59	-0.115	-0.03
31	Z1toZ3	-35.6	3.32	7.944	-35.6	3.323	3.75	##	-36	-0.193	1.58	0.590	0.60	-0.587	-0.60	-0.083	-0.06
32	Z1toZ3	-40.2	3.30	8.689	-40.2	3.302	3.72	##	-40	-0.117	1.82	0.609	0.62	-0.601	-0.61	-0.104	-0.09
33																	
34																	
35																	
36																	
37																	
38																	
39																	
40																	
41																	
42																	
43																	
44																	
45																	
46																	
47																	
48																	
49																	
50																	
51																	
52																	
53																	
54																	
55																	
56																	
57																	
58																	
59																	
60																	
61																	
62																	
63																	
64																	
65																	
66																	
67																	
68																	
69																	
70																	
71																	
72																	
73	m		-1.62E-01			6.94E-03			m	-5.35E-02		-3.35E-03		2.36E-03		6.44E-03	
74	b		2.17E+00			3.99E+00			b	-3.27E-01		4.86E-01		-5.20E-01		1.68E-01	

	DL	DM	DN	DO	DP	DQ	DR	DS	DT	DU	DV	DW	DX	DY	DZ
21															
22															
23	Z7	linZ7	Z8	linZ8	avgT	Z4	linZ4	Z5	linZ5	Z6	linZ6	Z7	linZ7	Z8	linZ8
24	-0.157	-0.15	-0.125	-0.20	-3.1	0.484	0.50	-0.533	-0.53	0.074	0.15	-0.157	-0.15	-0.125	-0.20
25	-0.119	-0.13	-0.163	-0.19	-9.1	0.485	0.52	-0.536	-0.54	0.063	0.11	-0.119	-0.13	-0.163	-0.19
26	-0.174	-0.11	-0.238	-0.19	-13.6	0.564	0.53	-0.488	-0.55	0.099	0.08	-0.174	-0.11	-0.238	-0.19
27	-0.134	-0.10	-0.255	-0.18	-16.6	0.565	0.54	-0.459	-0.56	0.130	0.06	-0.134	-0.10	-0.255	-0.18
28	0.095	-0.08	-0.240	-0.18	-21.4	0.602	0.56	-0.841	-0.57	0.206	0.03	0.095	-0.08	-0.240	-0.18
29	-0.090	-0.07	-0.163	-0.17	-26.7	0.439	0.58	-0.512	-0.58	-0.026	0.00	-0.090	-0.07	-0.163	-0.17
30	-0.151	-0.05	-0.129	-0.17	-30.2	0.691	0.59	-0.584	-0.59	-0.115	-0.03	-0.151	-0.05	-0.129	-0.17
31	0.006	-0.03	-0.137	-0.16	-35.6	0.59	0.60	-0.587	-0.60	-0.083	-0.06	0.006	-0.03	-0.137	-0.16
32	-0.026	-0.02	-0.153	-0.16	-40.2	0.609	0.62	-0.601	-0.61	-0.104	-0.09	-0.026	-0.02	-0.153	-0.16
33															
34															
35															
36															
37															
38															
39															
40															
41															
42															
43															
44															
45															
46															
47															
48															
49															
50															
51															
52															
53															
54															
55															
56															
57															
58															
59															
60															
61															
62															
63															
64															
65															
66															
67															
68															
69															
70															
71															
72															
73	-3.62E-03		-1.01E-03			-3.35E-03		2.36E-03		6.44E-03		-3.62E-03		-1.01E-03	
74	-1.62E-01		-2.00E-01			4.86E-01		-5.20E-01		1.68E-01		-1.62E-01		-2.00E-01	

FIGURE 9

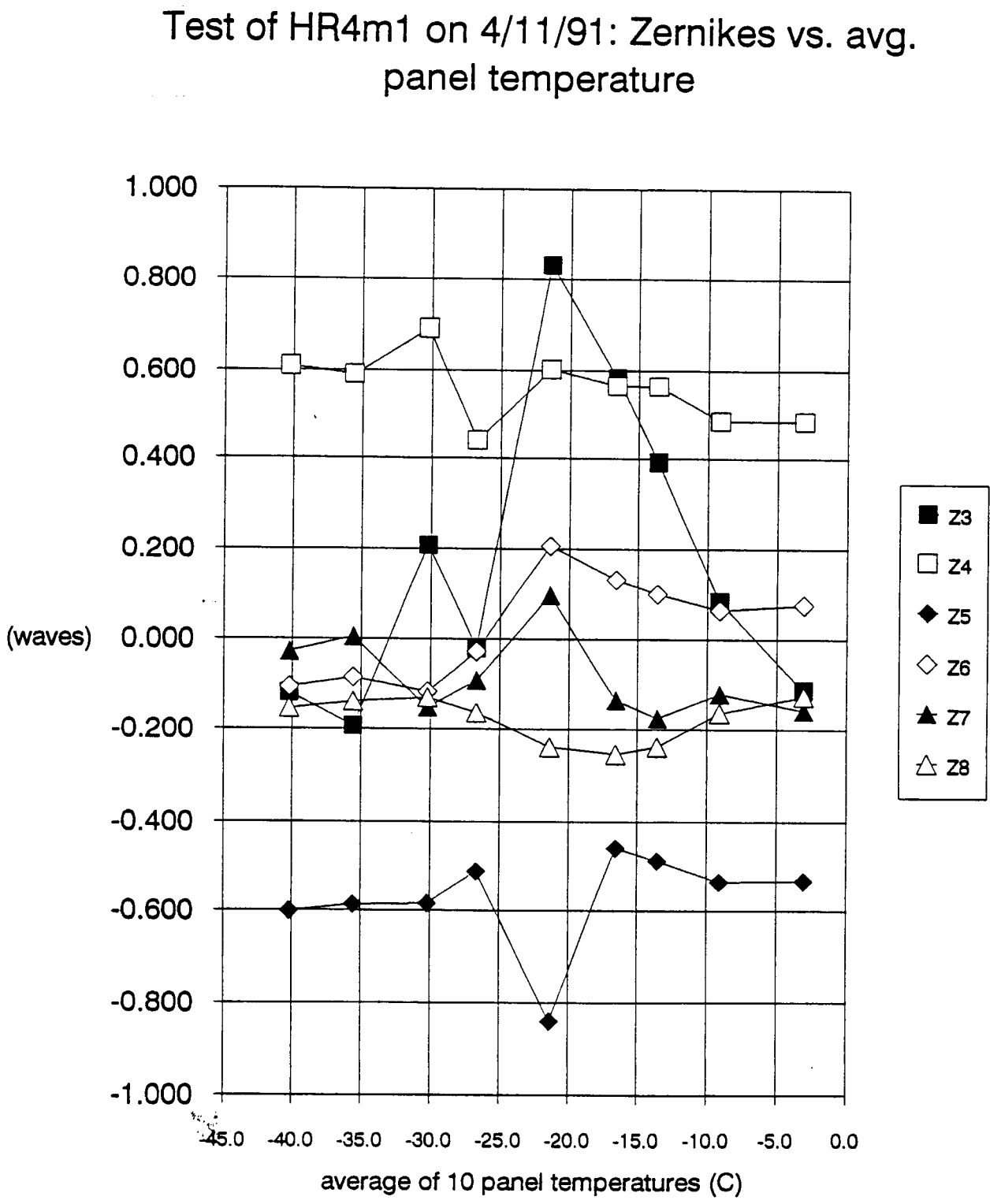
Test of HR4m1 on 4/11/91: Zernikes vs. avg. panel temperature
1.000
0.800
0.600
0.400
0.200
0.000
-0.200
-0.400
-0.600
-0.800
-1.000
(waves)
-45.0
-40.0
-35.0
-30.0
-25.0
-20.0
-15.0
-10.0
-5.0
0.0
average of 10 panel temperatures (C)
Z3
Z4
Z5
Z6
Z7
Z8

FIGURE 10

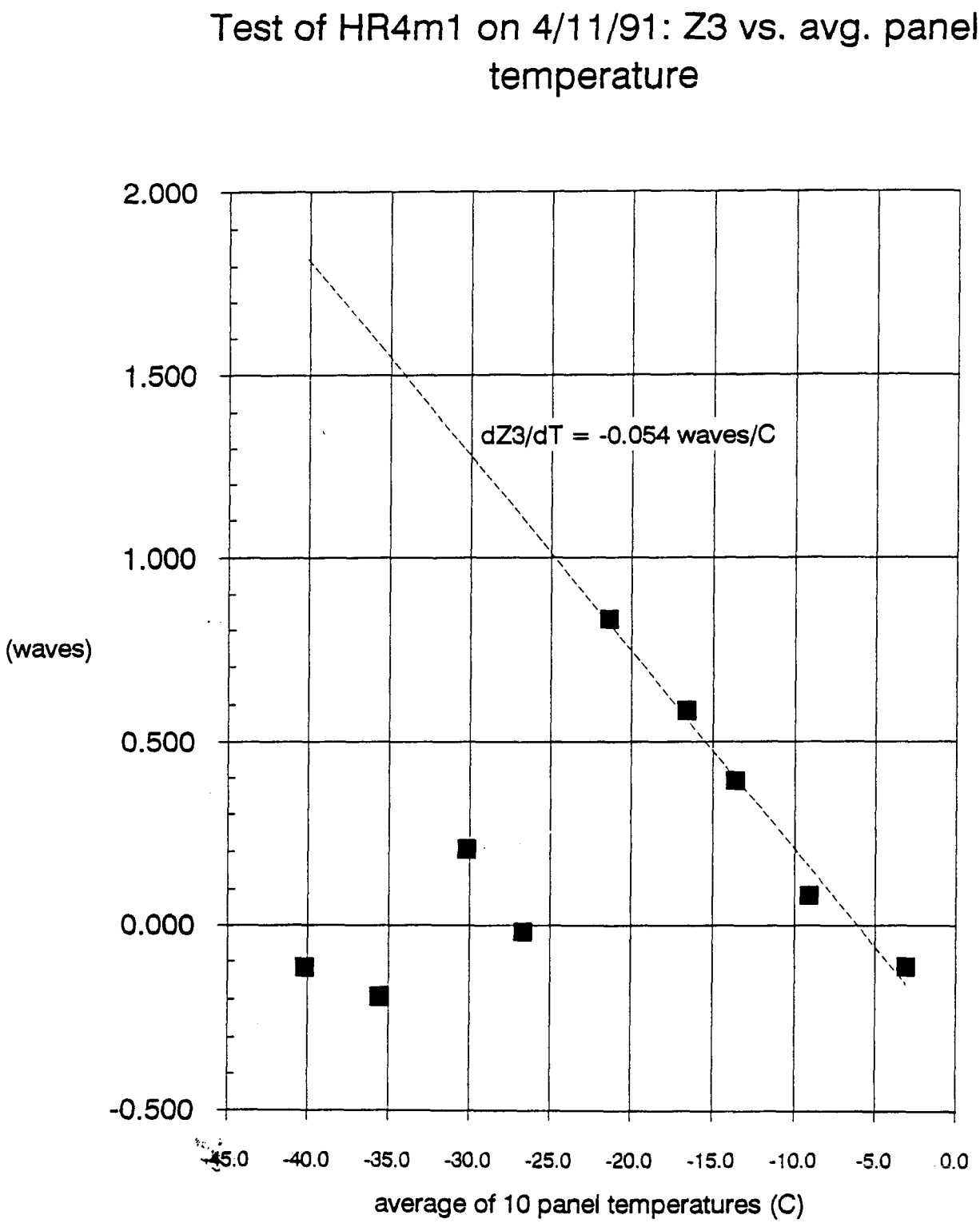
Test of HR4m1 on 4/11/91: Z3 vs. avg. panel temperature
2.000
1.500
1.000
0.500
0.000
-0.500
(waves)
dZ3/dT = -0.054 waves/C
-45.0
-40.0
-35.0
-30.0
-25.0
-20.0
-15.0
-10.0
-5.0
0.0
average of 10 panel temperatures (C)

FIGURE 11

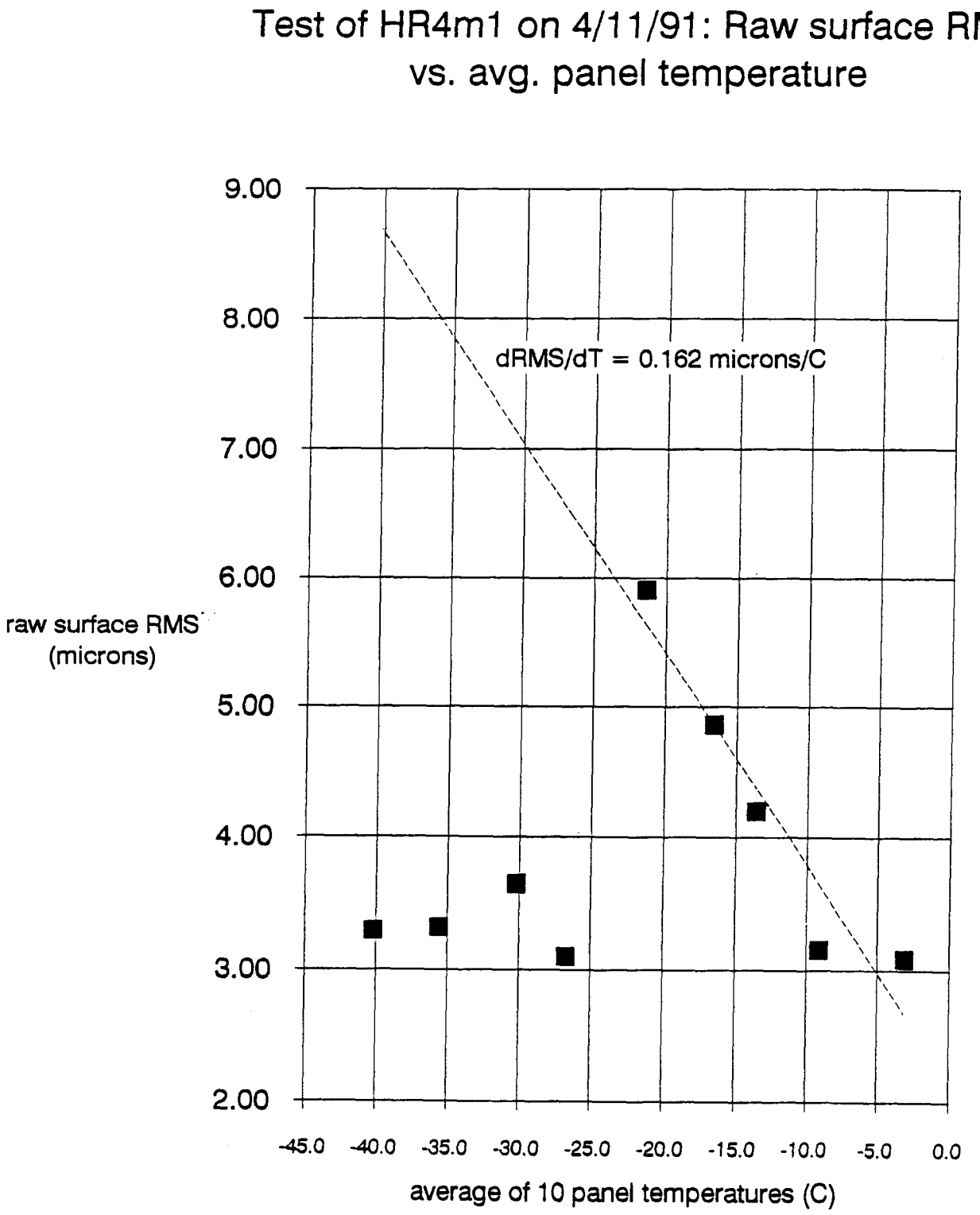
Test of HR4m1 on 4/11/91: Raw surface RMS vs. avg. panel temperature
9.00
8.00
7.00
6.00
5.00
4.00
3.00
2.00
raw surface RMS (microns)
dRMS/dT = 0.162 microns/C
-45.0
-40.0
-35.0
-30.0
-25.0
-20.0
-15.0
-10.0
-5.0
0.0
average of 10 panel temperatures (C)

Figure 12: PANEL TOTAL RMS THERMAL STABILITY